An investigation into the relationship between air temperature and the speed of sound through resonant frequency

Extended Essay: PHYSICS

To what extent can one both affordably and accurately measure the variation of the speed of sound in a column of dry air as air temperature changes through investigation in the context of resonance?

Word Count: 3997

Acknowledgements

Before commencing, I must mention and express great gratitude to some of the people who made this investigation possible. Firstly, I would like to thank Mr Paul Hunter, physics teacher at the Queensland Academy for Science Mathematics and Technology (QASMT) and the school entity for allowing me to borrow and use, at-home, their RØDE NT5 Condenser microphone and QSC K10.2 loudspeaker. These two pieces of expensive equipment served as vitally important requirements for my experiment to be successful and as such, the generosity and trust of these two parties made my data analysis possible. I am further grateful for Mr Paul Hunter, who, as my extended essay supervisor and having experience in the area of acoustics and sound management, prompted me in the theoretical direction which would eventually allow me to turn my undeveloped interest in this essay's subject area into a reality. I would also like to acknowledge Dr Kirsten Hogg, physics teacher at QASMT, and provide my gratitude for her support in the process of creating this essay, since she not only lent me a copy of her book, *Measured Tones*, by Ian Johnson, who's writing became part of my inspiration and theoretical understanding for this research, but also gave up her time to help me in the drafting process to give this essay the most streamline and clear direction. Finally, I wish to thank my parents for their unconditional interest and support of my work throughout the period of months prior to this essay's completion.

TABLE OF CONTENTS

1 Research Question

To what extent can one both affordably and accurately measure the variation of the speed of sound in a column of dry air as air temperature changes through investigation in the context of resonance?

2 Introduction

2.1 Practical Applications

In sound generation, recording and music performance, room acoustic performance is as important as the instruments themselves. Acoustic performance is the room's ability to sustain sound frequencies at their desired intensities. This makes room tuning important, the deliberate amplification or dampening of certain frequencies to combat or support the room's natural acoustic signature - the pattern of frequencies it amplifies. This acoustic signature results from resonance, where an environment's geometric features inherently allow standing waves of certain frequencies, making them audibly louder.

The speed of resonating sound, of many factors, determines these frequencies, therefore being a popular scientific research subject. One of sound speed's most unpredictable influences is temperature. Since indoor concert halls often keep temperature constant, room tuning is rarely necessary. However, for spaces unable to regulate temperature, unintentional fluctuations change the space's acoustic signature, hindering performance quality. Thus, a quantitative study into temperature and sound speed would be valuable for mitigating undesirable resonance.

2.2 Personal Context

In my seven years of trombone playing, I have been intrigued by the need to fully retune my instrument after room temperature changes. It becomes flat or sharp as its internal acoustic signature changes. In this essay, I attempt to quantify temperature's impact of on resonance, the mechanism by which trombones produce sound. Unfortunately, similar previous experiments have been expensive, typically requiring specialist equipment or chambers to attain reliable results. More affordable experiments present benefits to society with increased accessibility, allowing us to test the proposed scientific procedure more rigorously. Hence, I attempt to accurately reproduce the known trend with my limited available resources.

3 Relevant Theoretical Concepts

3.1 Standing Waves, Superposition and Resonance

Resonance relies on standing waves, the continuous superposition of two identical travelling waves in opposing directions. The amplitude of the resultant wave at any point is the summation of the substituent wave amplitudes from equilibrium, as in Figure 3.1 (University of Tennessee, Department of Physics and Astronomy, 2020). This explains how resonance amplifies sound intensity.

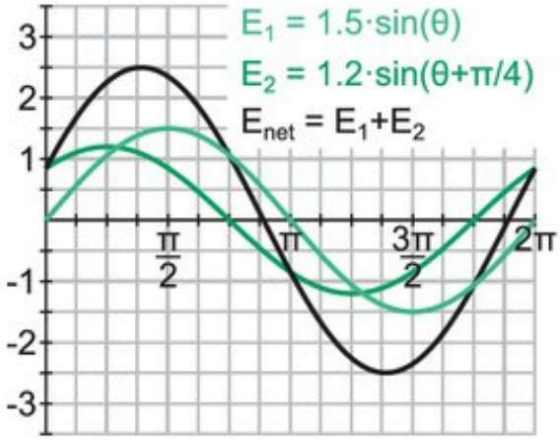

Figure 3.1: Principle of superposition as demonstrated by the summation of two sinusoidal functions (Ellis, 2014)

3.2 Resonant Harmonics in Tubes

Resonance is often observed in tubes by stimulating a column of air. Resonant frequencies are known as the tube length-dependent harmonics. Figure 3.2 shows a one open-ended tube's first and third standing wave harmonics (one open-ended harmonics are only odd). In resonance, sound's wavelength must create a node (continual destructive interference) at the closed end and an antinode (maximum amplitudinal fluctuation) at the open end (Tsokos, 2014). The wavelength, λ_n, of the n^{th} harmonic, in an L length one open-ended tube, equals $\lambda_n = \frac{4L}{n}$ $\{n =$

$1, 3, 5, \dots\}$ (Tsokos, 2014). Substituting $\frac{v}{f}$ for λ from the wave speed equation, $v = \lambda f$, means the n^{th} harmonic frequency becomes $f_n = \frac{vn}{4L}\ \{n = 1, 3, 5, \dots\}$ (Georgia State University, Department of Physics and Astronomy, 2016). Also, the tube's thermal expansion will be assumed negligibly small in this experiment (Mitra & Joshi, 1961).

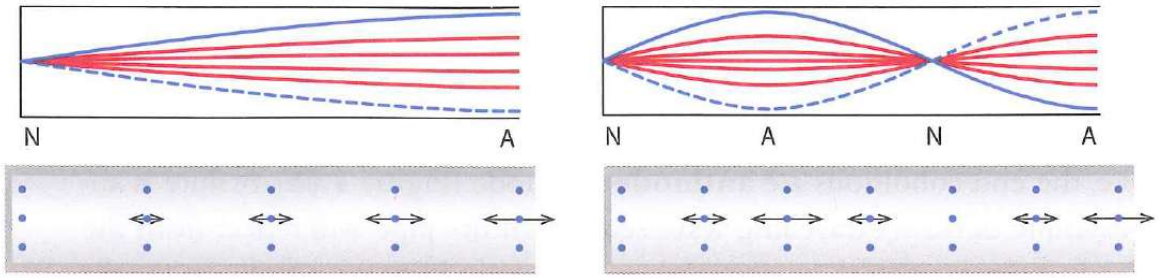

Figure 3.2: Illustration of first and third harmonics in a basic one open-ended tube system (Tsokos, 2014)

3.3 End Correction

From Figure 3.2, nodes exist at the closed end where air is stationary and antinodes at the open end where air pressure fluctuates. However, in practicality, pressure antinodes appears slightly past the tube's opening, by a distance called the end correction. Thus, the tube's effective length is longer than measured length, as in Figure 3.3 (Campbell, 2001). End correction is known to be directly proportional to hydraulic diameter. While many experimental methods have also existed, multiple mathematical approaches have found it reproducibly as $C = 0.30665D_h$, where C is the tube's end correction and D_h is its hydraulic diameter (Dalmont, Nederveen, & Jolly, 2001) (Schwinger & Levine, 1948). So, this calculation was used in this essay. Hydraulic diameter (D_h), often referenced in the study of flow, is simply internal diameter, as in Figure 3.4, spanning the area with potential to contain air (Atkins & Escudier, 2013).

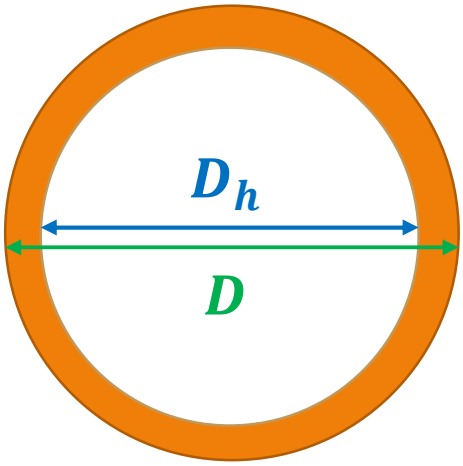

Figure 3.4 (left): Cross-section of tube demonstrating hydraulic vs. external diameter

Figure 3.3 (right): Illustration of an open-ended tube's end correction (Boelkes & Hoffmann, 2011)

3.4 Speed of Sound as a Function of Temperature

The predictable trend of temperature's impact on air density and average random kinetic energy of air particles is well-documented. As temperature rises, the speed of sound in air increases (Worland & Wilson, 1999). A function was found experimentally which approximates this trend in dry air within 250K and 335K, when air at atmospheric pressure may be treated as an ideal gas (Bacon, 2012) (Bacon & Torok, 2011):

$$v \approx 331.3\left(1+\frac{T_C}{273}\right)^{1/2};$$

v is the speed of sound in metres per second and T_C is the air temperature in degrees Celsius. This is also often approximated to $v \approx 0.6T_C + 331.4$ (Georgia State University, Department of Physics and Astronomy, 2016).

4 Relevant Practical Concepts

The following concepts and topics were crucial considerations in the decision-making to formulate this experimental design.

4.1 Input and Output Frequency Response

In the acoustics industry, frequency response curves illustrate the acoustic identity of microphones and speakers by identifying their sensitivity or bias towards specific frequencies when recording or playing respectively (Rochman, 2017). Flat responses, such as Figure 4.1, lack an intensity bias, while tailored responses favour some frequencies over others, such as human vocal range frequencies for a vocal microphone. The inherent relative intensity of frequencies for speakers is vitally important for specialist speakers such as subwoofers, tailored to the base end of human audibility (United States of America Patent No. US7003124B1, 2006).

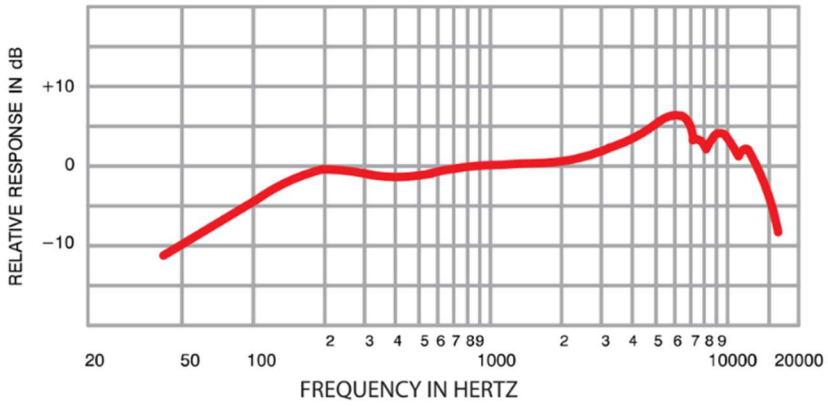

Figure 4.1: Flat microphone frequency response curve (Rochman, 2017)

4.1.1 White Noise

White noise is usually used to identify frequency response curves. This is sound with uniform energy across all frequencies between 20Hz and 20000Hz, only playable by perfectly flat response speakers (Butterfield & Szymanski, 2018). White noise provides "broadband tonal excitation", rather than one frequency's "pure tone excitation", meaning the relative input or output intensity of white noise is a microphone or speaker's frequency response (Abom & Allam, 2006). This has scientific applications, such as in Pushkarna's 2017 end correction study, in locating a tube's fundamental frequency (first harmonic).

4.2 Microphone Polar Patterns

Microphone design features frequency sensitivity, but also directional sensitivity, indicated by a polar pattern (Gallagher, 1999). Every polar pattern is a variation of the omnidirectional, cardioid, or bidirectional in Figure 4.2, Figure 4.3, and Figure 4.4, respectively. The further the radius is from the microphone head, the more directionally sensitive the microphone is. Many polar patterns are represented by two-dimensional rotary graphs of angle against intensity.

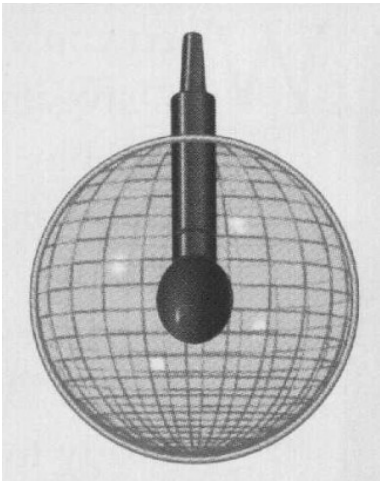

Figure 4.2: Polar pattern of an omnidirectional microphone (Gallagher, 1999)

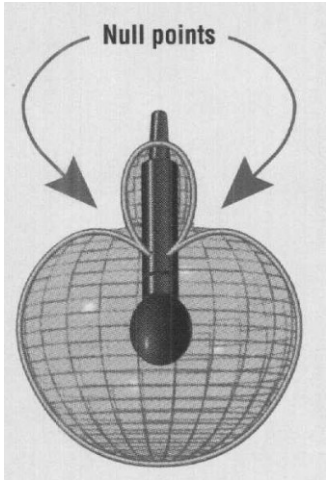

Figure 4.3: Polar pattern of a cardioid microphone (Gallagher, 1999)

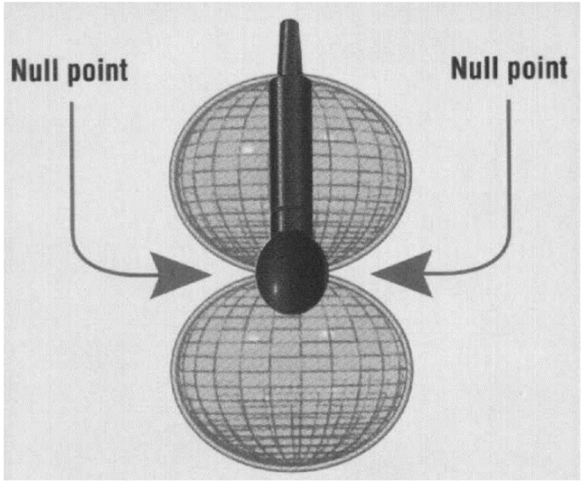

Figure 4.4: Polar pattern of a bidirectional microphone (Gallagher, 1999)

4.3 Architectural Acoustics

Ian Johnston (2009) writes in *Measured Tones*: “rooms aren’t exactly musical instruments, but they do affect the sound of any music played inside them”, emphasising the importance of room tuning. Sound energy can either be reflected from or absorbed by barriers. Geometric reverberation is repeated reflection, as in Figure 4.5. While reverberance is sometimes necessary, when testing the acoustic signature of equipment, it is a liability. Thus, measures exist to limit sound reflection.

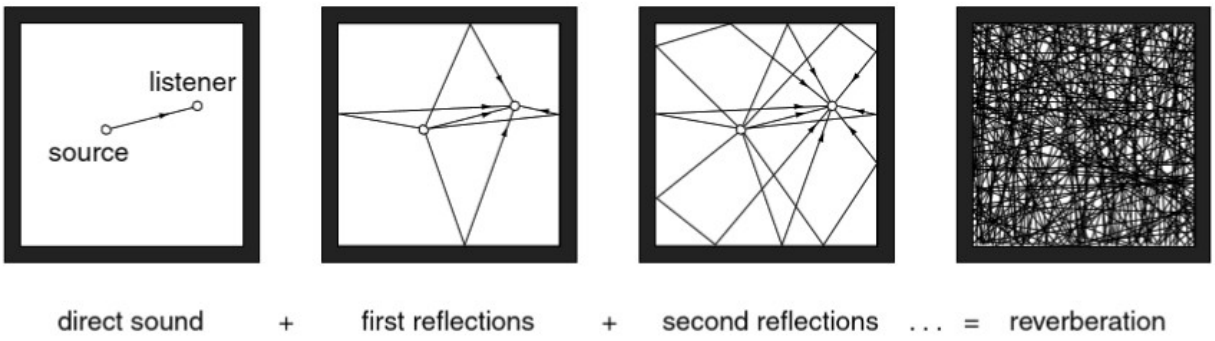

Figure 4.5: Reflections becoming reverberance in room due to lack of sound absorption (Johnston, 2009)

4.3.1 Anechoic Chambers

Anechoic chambers minimise reverberance by absorbing sound energy, where chamber walls have an “absorption coefficient [of] at least 0.99 for all angles of incidence”, being the proportion of sound that is absorbed (Kuttruff, 2016). However, Kuttruff notes that even absorption coefficients of 0.90 make an environment seem acoustically ‘dry’. It is also not sufficient for chamber walls to have an instantaneous transfer from air to a sound-absorbent material like polyurethane foam, needing a gradual shift, often with protruding foam wedge shapes as in Figure 4.6. Pragmatically speaking, the wedge length should be at least one third of the incident sound’s wavelength (Kuttruff, 2016). Anechoic chambers provide two main benefits for acoustic

experiments: 1) absorbing sound energy, reducing reverberation and; 2) minimising sound collisions with other anomalous objects, from generally uniform chamber design.

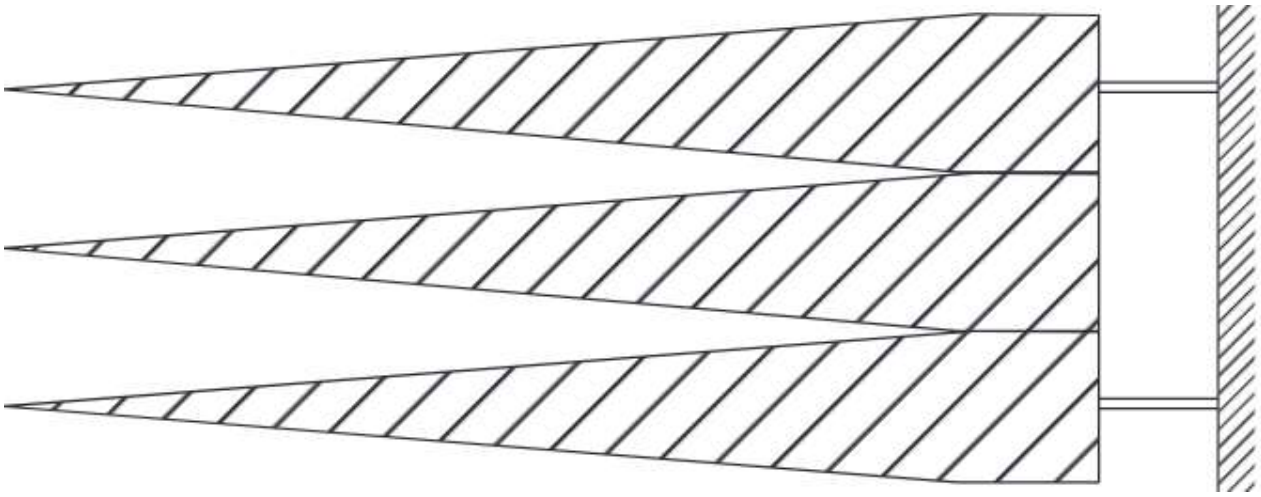

Figure 4.6: Simple repeating foam wedge design for anechoic rooms (Kuttruff, 2016)

5 Experimental Design

An experiment was designed which could determine the resonant frequencies of a constant length of steel tube reliably in a range of temperatures. Figure 5.1 and Table 5.1 present the equipment utilised.

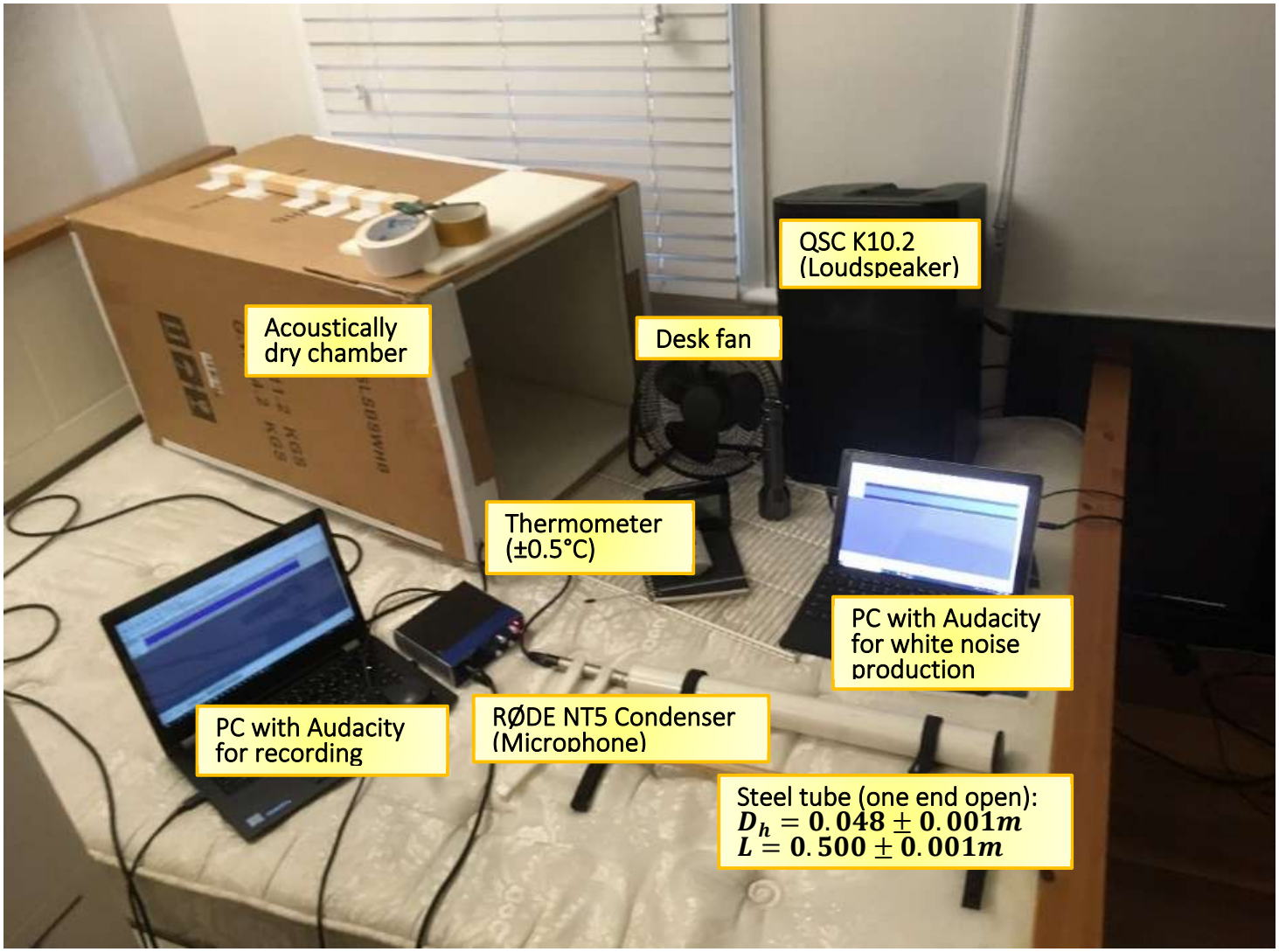

Figure 5.1: Visual equipment article list

Table 5.1: Unlisted experimental equipment items

Article
Digital air conditioner (18.0°C-30.0°C range of 1°C increments)
Handheld hair dryer
8°C industrial refrigerator

5.1. Experimental Procedure Outline

This experiment recorded, with a microphone, a tube's response to white noise from a loudspeaker, at different in-tube air temperatures. At each temperature, two chamber sound samples were taken with and without the tube giving two trials. The tube was hung in the chamber by foam tape to not dampen resonance. The microphone was positioned at the opening of the tube without entering to avoid internal reverberation while maintaining focus on the tube's response, as in Figure 5.2. For calibration, it was noted prior to tests that the internal chamber seemed acoustically 'dry'.

Figure 5.2: Microphone hung in front of the tube

Figure 5.3: External view of chamber opening

As in Figure 5.3, the chamber was open during each test to accommodate the loudspeaker at the opening. An air conditioner adjusted the room temperature from 18.0°C to 30.0°C in 2.0°C increments, with the analogue thermometer (±0.5°C) to confirm the in-tube air temperature. A fan circulating in the chamber assisted in reaching thermal equilibrium quickly but was turned off during tests to eliminate pressure disturbances. For the 32.0°C and 34.0°C readings, a hair dryer directly heated the tube, using the thermometer once again. For an 8.0°C anomalous temperature test, the apparatus was relocated and operated in an industrial refrigerator.

5.2 Experimental Design Choices

Various key decisions helped attain the most reliable results possible, in the limits of resource availability.

5.2.1 Acoustically Dry Chamber

An acoustically dry chamber, of cardboard and foam, was constructed and used like an anechoic chamber without the high cost (Kuttruff, 2016). While not being definitionally anechoic, the chamber maintained constant tube positioning to make reverberation consistent, which otherwise would reflect from objects and furniture. It also enhanced sound absorption, seeming more acoustically dry than the surroundings.

5.2.2 Frequency Response of Input/Output Devices

In Figure 5.4, a pilot test with a vocal microphone and small speaker was conducted. However, the data set was skewed as the speaker favoured higher frequencies and the microphone prioritised the vocal range. To combat this, a QSC K10.2 (loudspeaker) and RØDE NT5 Condenser (microphone) were chosen for their distinctively flat frequency responses in Figure 5.5 and Figure 5.6 respectively (Studiospares Europe Ltd, 2020) (Crutchfield New Media, LLC., 2020). The limitations in their flat curves formed this experiment's boundary frequencies.

5.2.3 Microphone Polar Pattern

Figure 5.6 provides the RØDE NT5 Condenser's cardioid polar pattern. This monodirectional microphone ensured focus on the tube's response and not the speaker's projection.

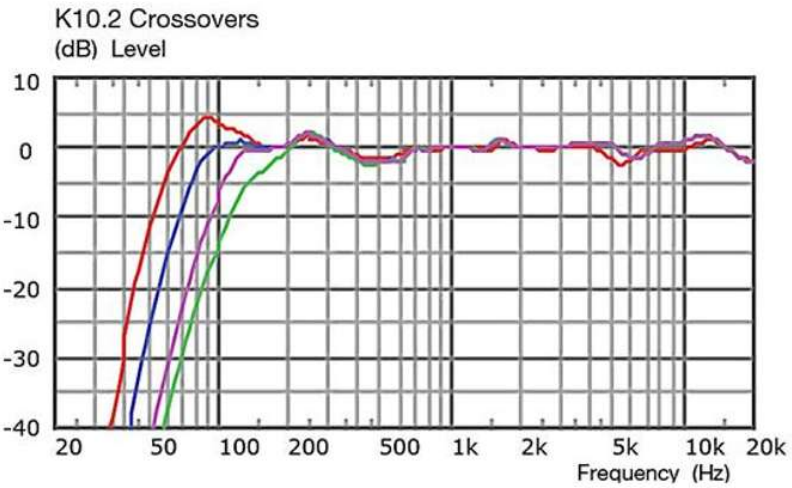

Figure 5.5: Frequency response curve for QSC K10.2 loudspeaker (Crutchfield New Media, LLC., 2020)

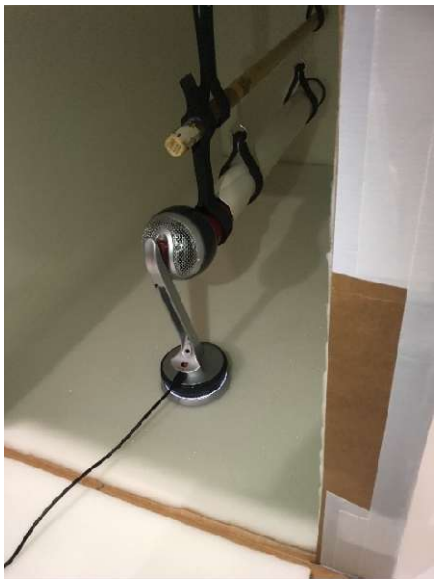

Figure 5.4: Initial tailored frequency response experiment design

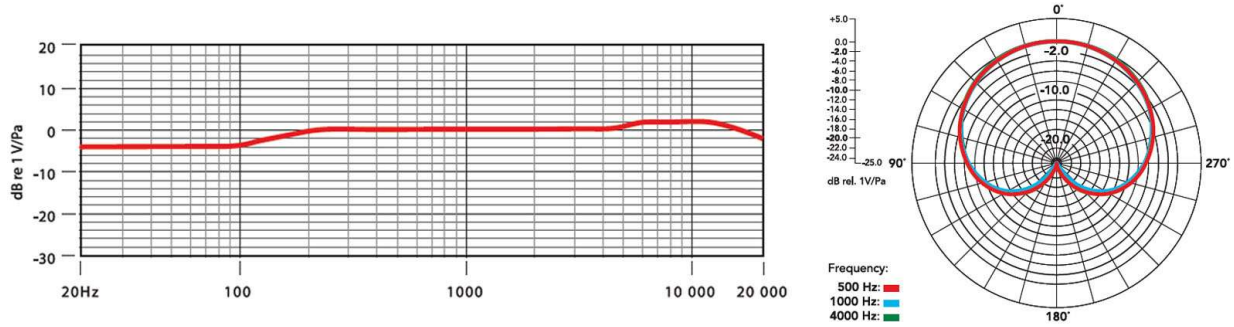

Figure 5.6: Frequency response curve for RØDE NT5 Condenser microphone (Studiospares Europe Ltd, 2020)

5.3 Data Collection

Each test recorded 15 seconds, but only the central 10 seconds were analysed, allowing 2.5 seconds on either side for external noise in preparation. Data was then presented as a frequency analysis, through the program Audacity, by plotting the relative intensity of all frequencies detected by the microphone.

5.4 Risk Assessment

There were no perceived economic, environmental, or ethical risks in this experiment. Some personal safety risks included: long-exposure to high frequencies; long-exposure to abnormal temperature and; musculoskeletal skeletal injury from manual handling of heavy electrical equipment. However, these were mitigated by: using the lowest speaker volume setting; wearing temperature-appropriate clothing; maintaining care and attention and; discontinuing trials immediately as symptoms are felt.

6 Experimental Results

6.1 Raw Frequency Analysis Data

Figure 6.1 and Figure 6.2 provide the frequency analysis graphs for the first 22.0°C trial without and with the tube, respectively. This particular trial is used for all sample calculations for continuity.

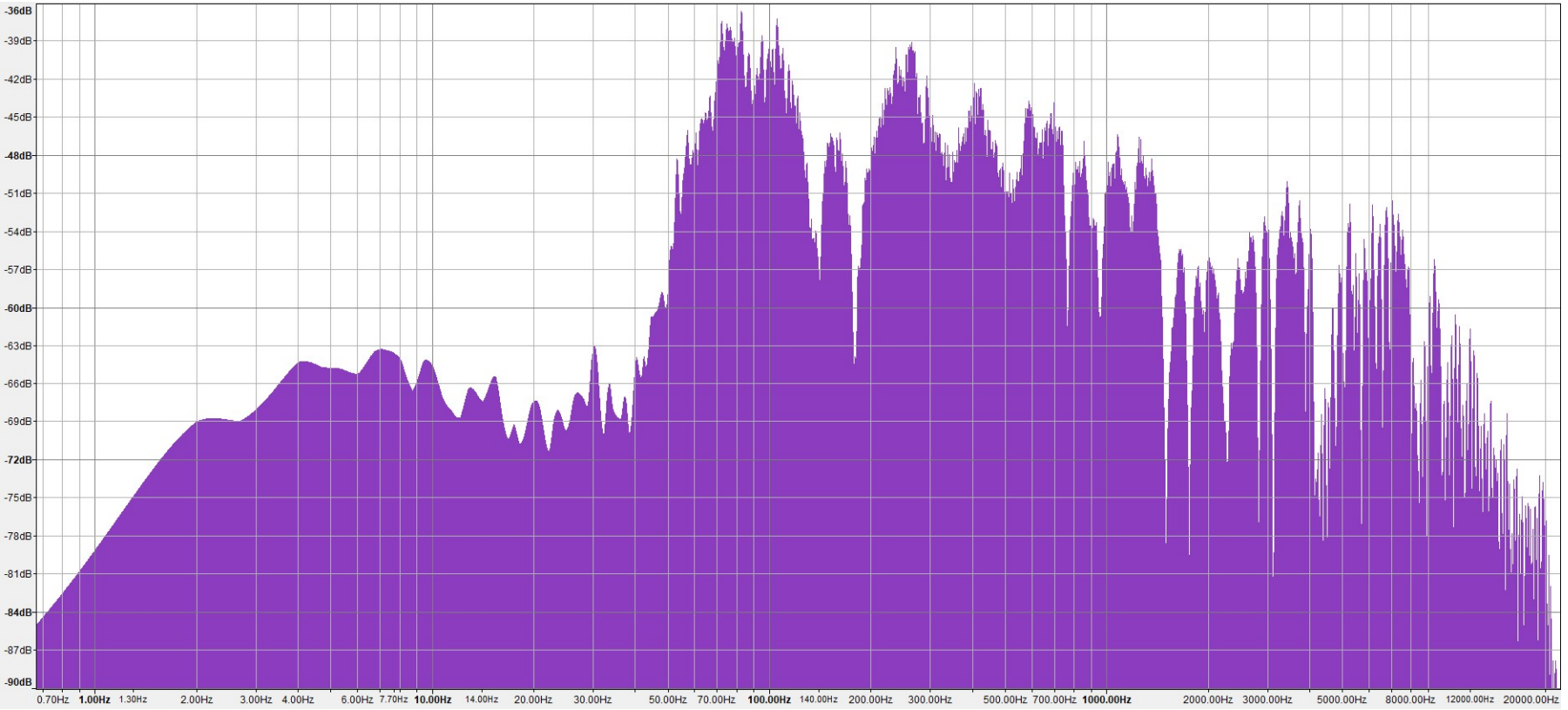

Figure 6.1: Raw logarithmic frequency analysis graph for the first trial of the 22.0°C white noise response without tube inserted (Audacity, 2020)

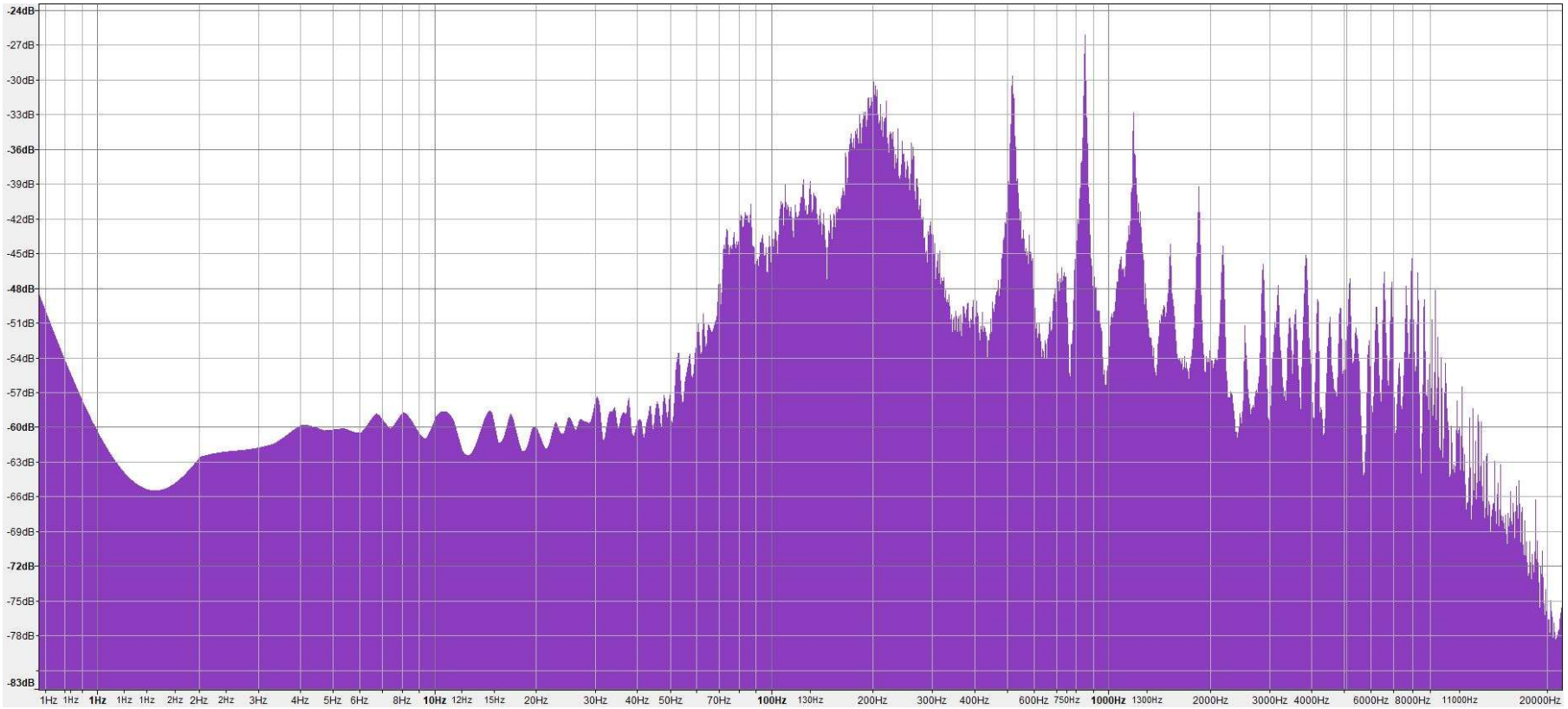

Figure 6.2: Raw logarithmic frequency analysis graph for the first trial of the 22.0°C white noise response with tube inserted (Audacity, 2020)

6.2 Data Focusing and Preparation

The first data preparation step is to focus solely on the tube's impact. The only change between Figure 6.1 and Figure 6.2 was the tube's insertion, so the vertical difference in intensity of each frequency between the curves quantifies the tube's impact alone. Figure 6.3 shows this subtracted curve of Figure 6.1 from Figure 6.2. From the equations: $f_n = \frac{vn}{4L}\ \{n = 1, 3, 5, \dots\}$ and $v = 331.3\left(1 + \frac{T_C}{273}\right)^{1/2}$; the seventh harmonic ($n = 7$) of a 0.5m tube at 34.0°C should only be approximately 1229.6Hz, so only the 0Hz to 1500Hz interval data was processed.

6.3 Peak Identification

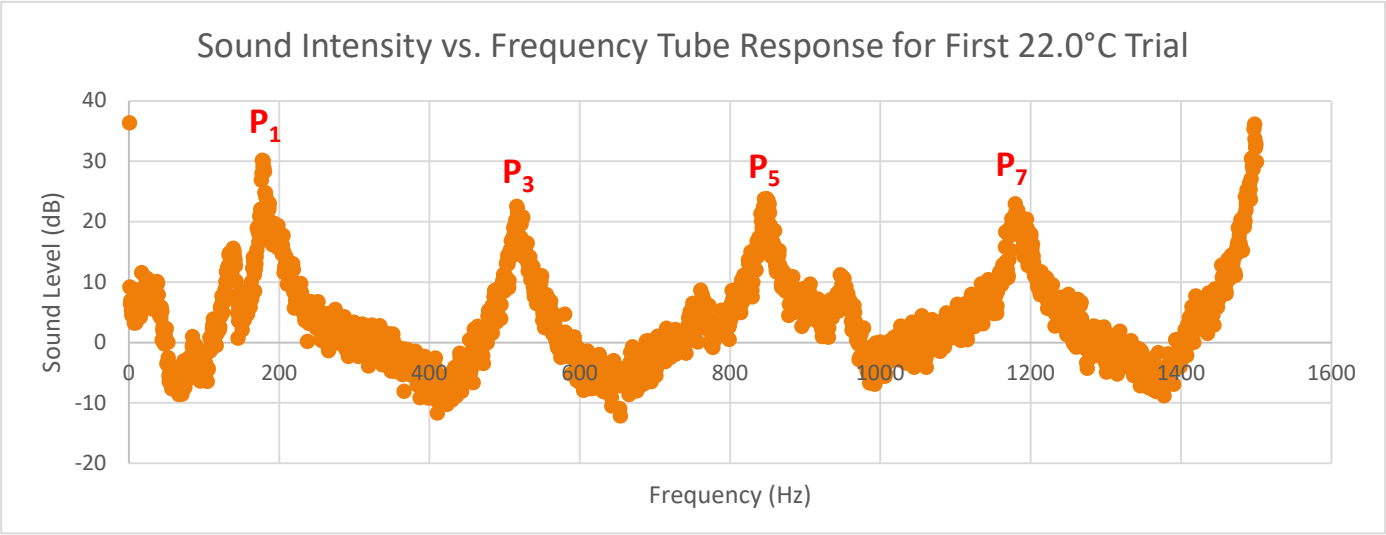

Figure 6.3: Frequency response of isolated tube across 4 harmonic theoretical range for the first 22.0°C

Figure 6.3 shows noticeable intensity peaks after the tube's insertion, representing resonant frequencies. Using $f_n = \frac{vn}{4L}\ \{n = 1, 3, 5, \dots\}$, it was found that $f_n = nf_1$. From the distinctive marked peaks, P_3 appears at a frequency location approximately 3 times that of P_1. This scalar multiple trend recurs for P_5 and P_7. From this evidence, including that P_1 is the graph's first noticeable peak, it is likely that P_1, P_3, P_5 and P_7 represent the resonant frequencies f_1, f_3, f_5 and f_7, respectively. The harmonic frequencies were cited as the frequencies of highest intensity.

6.3.1 Uncertainty Estimation

Audacity does not provide a tool error for the peak frequencies. Instead, a variation of Pushkarna's 2017 peak uncertainty derivation was used, who performed a similar process with Audacity. Pushkarna believed a more definitive peak to be a better-defined peak (Pushkarna, 2017). Thus, higher proximity line gradients (lines approaching and leaving the peak frequency) warranted lower uncertainties. Following this, Pushkarna's peak uncertainty was the product of the reciprocal of the mean of the proximity line gradients with a quantity called peak width. Pushkarna defined peak width as the frequency difference between the fourth point after and before the peak. Peak width was constant for all peaks as Audacity's frequency measurements have equal increments.

However, unlike Pushkarna's study, this experiment identified multiple peaks (different harmonics) in each temperature. It cannot be assumed that the proximity line gradients of two equally accurate harmonics would be the same, thus Pushkarna's method would attribute differing peak position uncertainties. Hence, this essay used the alternative coefficient of determination (R^2 value) quantity for proximity lines. This claims that higher proximity line R^2 values (more confident trends), foster lower uncertainties. This essay features direct substitution of R^2 for gradient in Pushkarna's method, meaning the absolute uncertainty (Δf_n) in peak f_n's position with proximity lines $L1$ and $L2$ is:

$$\Delta f_n = \frac{1}{mean(R_{L1}^2, R_{L2}^2)} \times (peak\ width) = \frac{2}{R_{L1}^2 + R_{L2}^2}\left(f_{upper} - f_{lower}\right)$$

Figure 6.4 provides a graphical sample calculation of the first harmonic in the first 22.0°C trial, found as 177.6±6.8Hz. Interestingly, since the reciprocal mean term in the uncertainty equation approaches 1 at high R^2 values, peak width is the peak position's lower bound. Since this procedure is not rigorously supported, one individual point's uncertainty may not be accurate. However, its merit is its consistency across points, so comparing uncertainties of many points will correctly gauge relative accuracy.

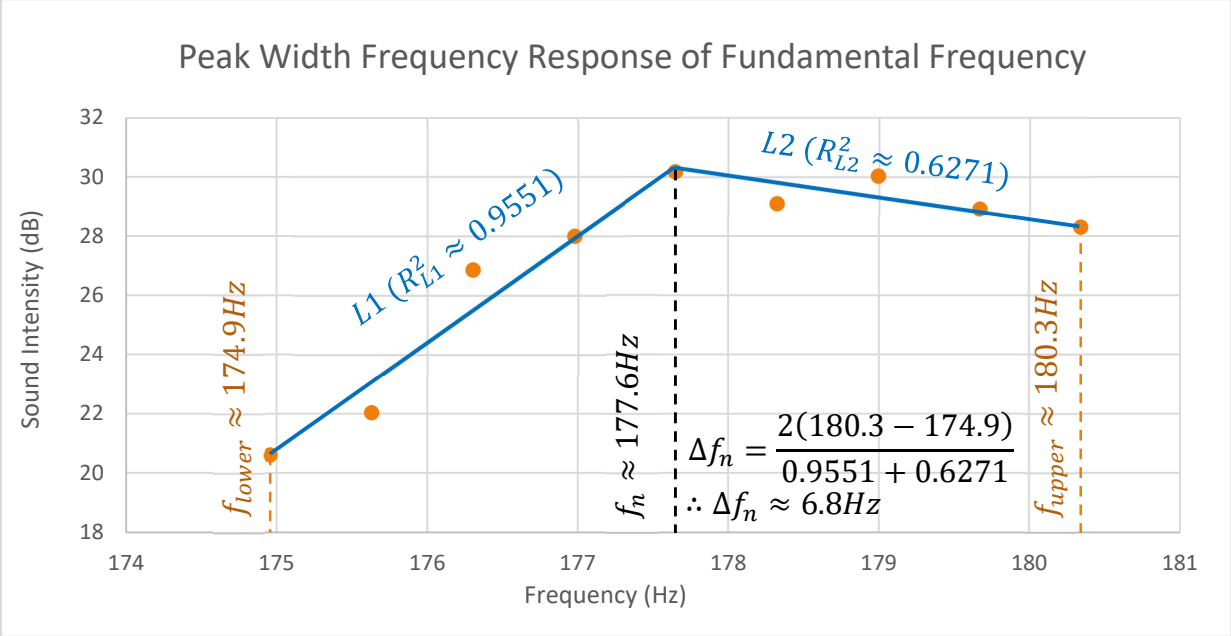

Figure 6.4: Illustration of peak width for uncertainty calculation of the first harmonic frequency of the first 22.0°C trial

7 Data Processing

This peak identification and uncertainty estimation was repeated for the first four harmonics of both trials and for all temperatures, giving Table 7.1. All values were rounded to one decimal place, the limit of reading for Audacity. Δf_n notates the absolute uncertainty of f_n.

Table 7.1: n=1,3,5,7 harmonic frequencies, with error estimation, from peaks identification of all temperature tests with two trials each

Temp. (±0.5°C)	Trial No.	f_1 (Hz)	Δf_1 $(\pm Hz)$	f_3 (Hz)	Δf_3 $(\pm Hz)$	f_5 (Hz)	Δf_5 $(\pm Hz)$	f_7 (Hz)	Δf_7 $(\pm Hz)$
8.0	1	161.8	7.2	508.7	7.9	829.7	8.3	1155.4	10.7
	2	163.4	9.3	509.1	5.9	829.3	9.6	1155.1	9.6
18.0	1	178.3	5.5	514.1	10.4	839.1	5.9	1173.6	11.8
	2	177.0	5.4	514.1	7.0	842.5	11.5	1164.8	6.8
20.0	1	178.3	5.5	521.5	10.3	854.6	7.4	1182.3	9.1
	2	178.3	6.2	514.1	9.2	849.2	11.9	1183.6	9.8
22.0	1	177.6	6.8	522.8	13.3	848.5	14.4	1179.6	13.8
	2	179.0	6.3	514.1	11.2	849.2	5.9	1183.7	11.9
24.0	1	179.0	12.8	520.8	12.6	851.9	6.5	1187.0	14.1
	2	179.7	14.4	520.2	21.2	849.9	11.0	1183.7	5.7
26.0	1	181.0	6.8	524.9	12.8	861.3	10.3	1191.1	7.5
	2	178.3	11.0	524.2	6.7	855.9	6.4	1189.7	11.2
28.0	1	181.7	6.7	523.5	8.9	859.3	6.5	1194.4	6.9
	2	181.7	11.7	525.5	7.4	861.3	6.6	1194.4	12.8
30.0	1	182.4	13.9	526.2	7.2	859.3	6.1	1200.5	7.5
	2	181.9	8.4	526.2	6.5	862.7	6.4	1197.1	8.3
32.0	1	181.0	9.0	530.9	7.6	864.7	9.0	1205.2	12.9
	2	183.7	10.0	527.6	10.3	862.0	8.0	1205.9	6.4
34.0	1	183.3	6.2	532.3	6.3	869.4	8.5	1211.9	8.3
	2	183.4	7.3	535.0	8.1	870.1	12.1	1209.9	9.1

7.1 Trial Averaging

To produce one coherent data set, the average of the two frequencies from each temperature and harmonic was taken by the equation: $\bar{x} = \frac{\sum_{i=1}^{n} x_i}{n}$; where $\bar{x}$ is the mean of all n values in the set x_i. To propagate the uncertainties of the averages, the following identity was utilised:

if $x = \frac{a \pm b}{n}$ $\{\Delta n = 0\}$, then $\Delta x = \frac{\Delta a + \Delta b}{n}$. Table 7.2 shows the averaged data set. Averages were once again rounded to one decimal place as the calculation does not yield accuracy.

Table 7.2: Averaged n=1,3,5,7 harmonic frequencies in each temperature, with error estimation

Temp. (±0.5°C)	f_1 (Hz)	Δf_1 $(\pm Hz)$	f_3 (Hz)	Δf_3 $(\pm Hz)$	f_5 (Hz)	Δf_5 $(\pm Hz)$	f_7 (Hz)	Δf_7 $(\pm Hz)$
8.0	162.6	8.3	508.9	6.9	829.5	9.0	1155.3	10.2
18.0	177.7	5.5	514.1	8.7	840.8	8.7	1169.2	9.3
20.0	178.3	5.9	517.8	9.8	851.9	9.7	1183.0	9.5
22.0	178.3	6.6	518.5	12.3	848.9	10.2	1181.7	12.9
24.0	179.4	13.6	520.5	13.4	850.9	8.8	1185.4	9.9
26.0	179.7	8.9	524.6	9.8	858.6	8.4	1190.4	9.4
28.0	181.7	9.2	524.5	8.2	860.3	6.6	1194.4	9.9
30.0	182.2	11.2	526.2	6.9	861.0	6.3	1198.8	7.9
32.0	182.4	9.5	529.3	9.0	863.4	8.5	1205.6	9.7
34.0	183.4	6.8	533.7	7.2	869.8	10.3	1210.9	8.7

7.2 Air Temperature vs. Resonant Frequency

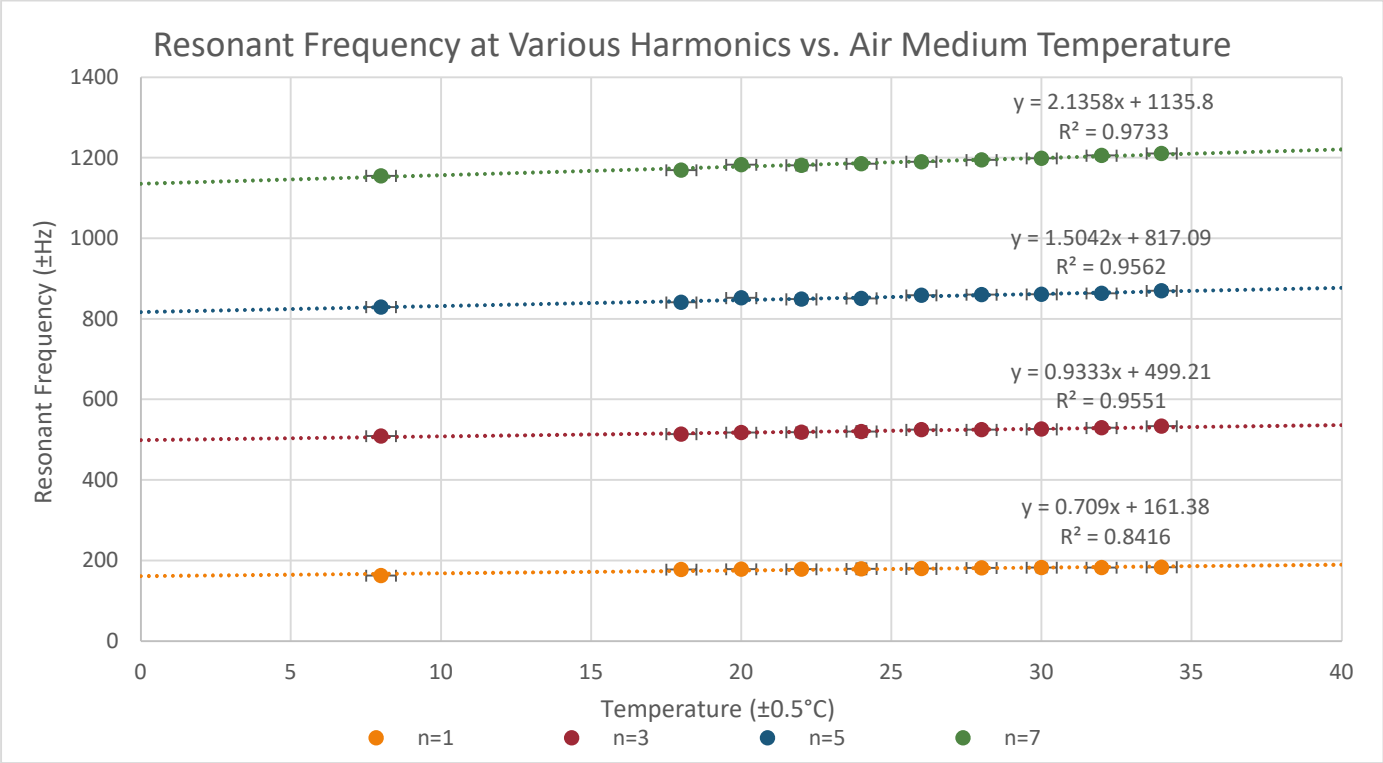

Figure 7.1: Graphical representation of the influence of temperature on the peak position of the n=1,3,5,7 harmonics

Figure 7.1 is a graph of Table 7.2, demonstrating how air temperature rises increase resonant frequency linearly from each curve's high R^2 value. Additionally, as the n value rose, the rate of change of resonant frequency with temperature increased, because with each harmonic as a multiple of the fundamental frequency, a first harmonic peak shift inspires larger movement for higher harmonics.

7.3 Speed of Sound Calculation

To transform this result into a trend for the speed of sound, the initial equation must be rearranged.

$$f_n = \frac{vn}{4L}\ \{n = 1, 3, 5, \dots\}, \qquad \therefore\ v = \frac{1}{n} 4L f_n$$

In this equation, L is the tube's effective length, as the sum of measured length and end correction. The end correction formula, $C = 0.30665 D_h$, with the tube's measured hydraulic diameter of 0.048±0.001m, gives the end correction as 0.0147±0.0006m. Hence, the effective length (L) was 0.5147±0.0016m.

Table 7.3 provides the data set of sound speed for each harmonic and temperature with propagated uncertainties. From $v = \frac{1}{n} 4Lf_n$, the relative uncertainties for L and v were found as the sum of all other relative uncertainties.

Table 7.3: Sound speed values with propagated uncertainties, calculated by n=1,3,5,7 harmonics in each temperature

Temp. (±0.5°C)	$v_{n=1}$ $(m \cdot s^{-1})$	$\Delta v_{n=1}$ $(\pm m \cdot s^{-1})$	$v_{n=3}$ $(m \cdot s^{-1})$	$\Delta v_{n=3}$ $(\pm m \cdot s^{-1})$	$v_{n=5}$ $(m \cdot s^{-1})$	$\Delta v_{n=5}$ $(\pm m \cdot s^{-1})$	$v_{n=7}$ $(m \cdot s^{-1})$	$\Delta v_{n=7}$ $(\pm m \cdot s^{-1})$
8.0	334.8	18.0	349.2	5.8	341.6	4.7	339.8	4.0
18.0	365.7	12.4	352.8	7.1	346.2	4.7	343.9	3.8
20.0	367.1	13.2	355.3	7.8	350.8	5.1	347.9	3.9
22.0	367.1	14.6	355.8	9.5	349.5	5.3	347.5	4.9
24.0	369.2	29.1	357.2	10.3	350.4	4.7	348.6	4.0
26.0	369.9	19.5	360.0	7.8	353.5	4.5	350.1	3.8
28.0	374.1	20.1	359.9	6.7	354.2	3.8	351.3	4.0
30.0	375.0	24.1	361.1	5.8	354.5	3.7	352.6	3.4
32.0	375.4	20.7	363.2	7.3	355.5	4.6	354.6	3.9
34.0	377.5	15.1	366.2	6.1	358.1	5.4	356.1	3.7

7.3 Graphical Display

Figure 7.2 provides a graph of Table 7.3, with sound speed curves for each harmonic.

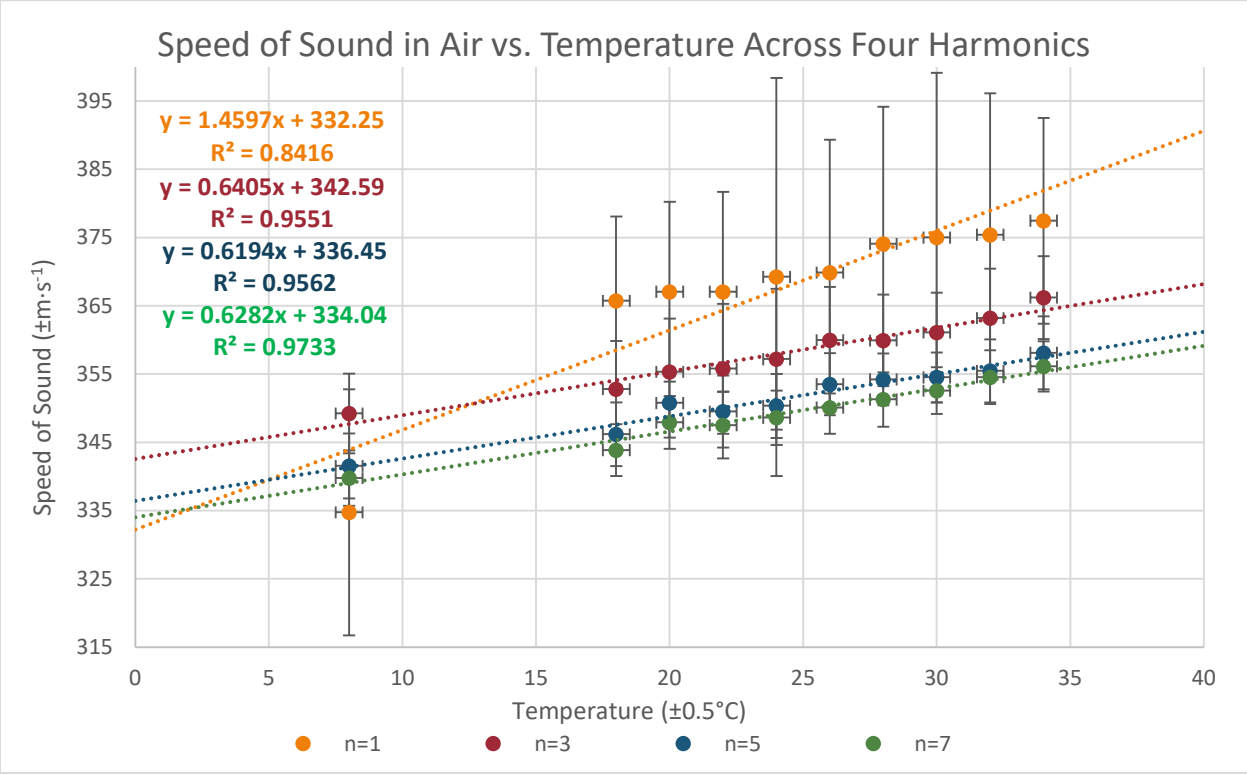

Figure 7.2: Graphical display of air temperature's effect on the speed of sound in the four harmonics

Importantly, each harmonic gives a different sound speed for one temperature. This was unexpected since a frequency change, which does not impact wave speed, is the only difference between harmonics (Georgia State University, Department of Physics and Astronomy, 2016). However, the trendlines may stem from a systematic error, as they are roughly parallel, being simply vertical shifts of each other.

8 Discussion

8.1 Outlier Removal and Literature Curve Comparison

To enforce this parallelism further, the 8.0°C first harmonic was omitted. This outlier offsets the $n = 1$ curve's gradient drastically, missing most horizontal error bars. Justification for this decision is detailed further in the evaluation. Figure 8.1 illustrates Figure 7.2 without this anomalous value, and including the literature curve for speed of sound in dry air against temperature in Celsius for comparison: $v = 331.3\left(1 + \frac{T_C}{273}\right)^{1/2}$ (Worland & Wilson, 1999).

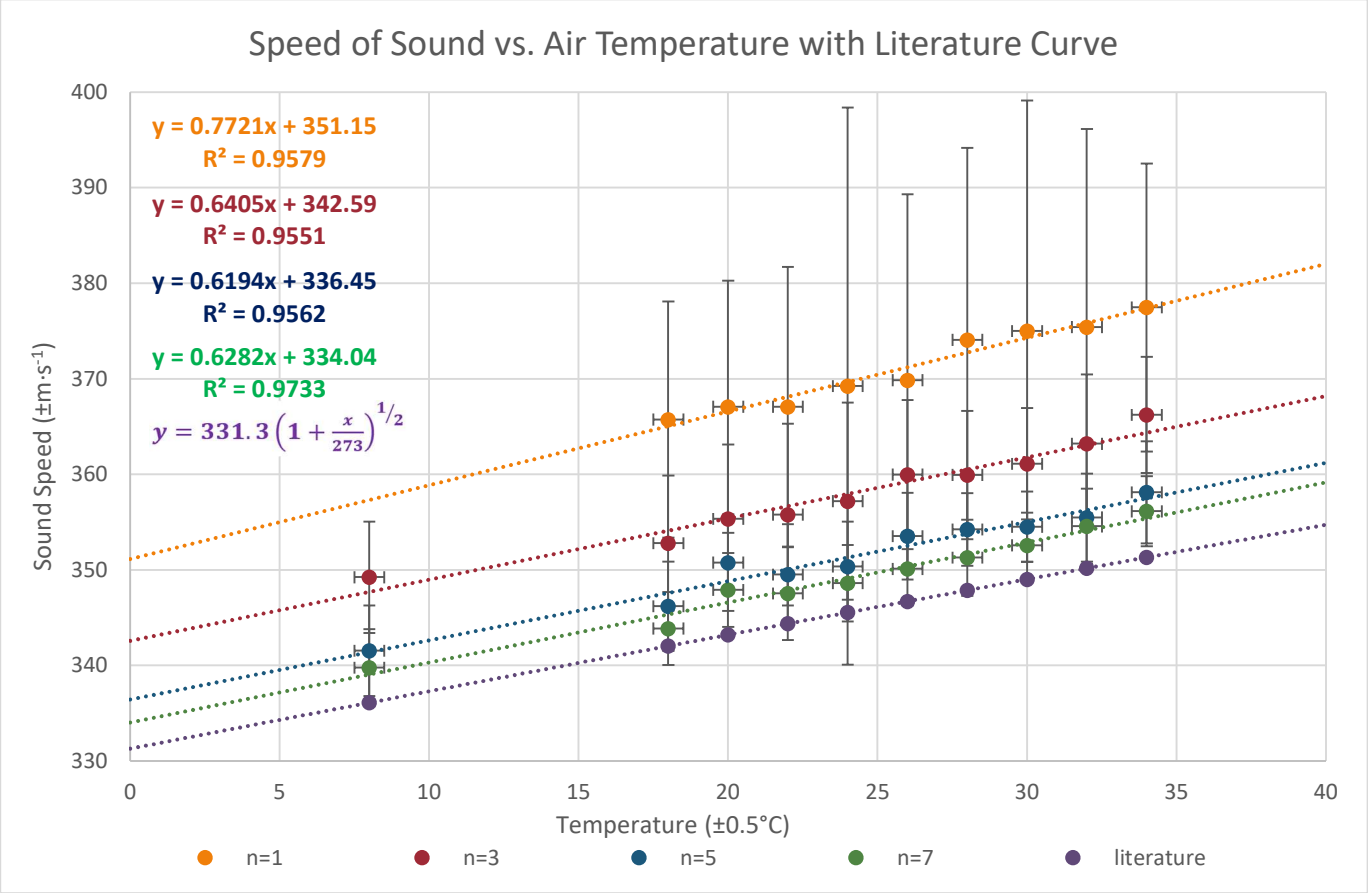

Figure 8.1: The impact of temperature on sound speed across four harmonics with a comparative literature curve

8.2 Graphical Interpretation

Now a more distinguishable trend is presented. Primarily, all R^2 values are greater than 0.95, indicating very strong linear correlations in the domain studied. Although the literature curve is a square root relationship, in this domain, it approximates the linear $v \approx 0.6T_{Celsius} + 331.4$ (Georgia State University, Department of Physics and Astronomy, 2016). With a linear literature curve, it becomes apparent that all trendlines possess gradients within the interval $0.6000m \cdot s^{-1} \cdot {}^{\circ}C^{-1} < m < 0.7721m \cdot s^{-1} \cdot {}^{\circ}C^{-1}$. The only significant deviation between the curves is their y-intercept, visibly decreasing as n value increases.

However, this does not explain the unexpected trend for the harmonics to possess separate trends. One possible explanation is due to the chamber's performance in different frequencies. While it demonstrated dry psychoacoustic properties, it did not possess the design of industrial anechoic chambers. Further, the fact an anechoic chamber's wedge length should be at least one third of the wavelength of absorbed sound suggests better performance at lower wavelengths and higher frequencies (Kuttruff, 2016). There is, thus, logical sense in how curves of higher n value (and sound frequency) had a closer proximity to the literature curve since low frequency analysis neglected reverberance that would not have been absorbed.

On this note, the rate of change of the y-intercept with respect to the n value is not constant, rather decreasing for higher n values. If this continued for even higher harmonics, then by the convergent sequence's definition: where $|u_{n+1} - u_{n+2}| < |u_n - u_{n+1}|$ when u_n is the n^{th} term in the sequence; the sound speed curve sequence as n increases would converge at an infinitely high n value (Lytle, 2015).

8.3 Convergence Test

Testing this theory, Figure 8.2 shows a plot of the 22.0°C sound speed against n value. The smart graphing tool, Desmos, found that the points were most accurately modelled by a simple graphical transformation of the reciprocal function: $y = \frac{a}{x} + b \; \{a, b \in \mathbb{R}\}$ (Desmos, Inc., 2020).

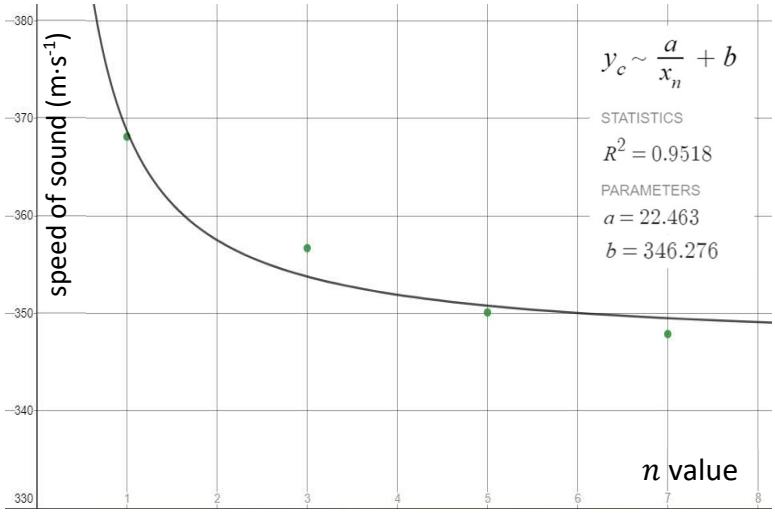

Figure 8.2: Test for graphical convergence of harmonics at 22.0°C (x-axis: harmonic n-value; y-axis: speed of sound at 22°C in m·s^{-1})

8.3.1 Graphical Significance of Reciprocal Function

With an R^2 value greater than 0.95, there is great certainty in the trend of Figure 8.2. Reciprocal functions converge as sequences at their horizontal asymptote $y = b = 346.276m \cdot s^{-1}$. This is the theoretical speed of sound at an infinitely high n value and frequency, hence when the chamber performs as a perfect anechoic chamber. When 22.0°C is substituted into the equation: $v = 331.3\left(1 + \frac{T_C}{273}\right)^{1/2}$; the speed $344.4m \cdot s^{-1}$ is found. With this as a literature convergent sound speed as n approaches infinity, the experimental value's percentage difference is approximately +0.54%; a remarkably accurate result. This conclusion is supported by the uncertainties of the Figure 8.1 curves, where the lower n value curves' points have larger uncertainties, matching their larger displacement from the literature curve.

This convergence testing could become an additional data processing step to find the most reliable sound speed value at each temperature, however, this would require the measurement of many more harmonics, whereas this experiment only found four. Yet, even without an anechoic chamber, this experiment has the potential for repetition, where frequency's relationship with chamber performance could accurately confirm the sound speed against air temperature trend with significantly lower expense than is traditional.

9 Evaluation

9.1 Potential Error Sources and Implications

Various unpredictable flaws in the procedure have potentially generated random and systematic error, impacting the data with point fluctuation and curve movement. The errors identified stem from temperature regulation and sound control.

Primarily, the anomalous 8.0°C first harmonic sound speed was questioned, previously neglected. In reality, it may indicate a deeper-rooted problem in how the study was approached: background noise. This was limited, however, during the 8.0°C industrial refrigerator, noise produced by food preservation equipment included a low rumbling fan. This lower-pitched external sound likely offset the first harmonic, causing the drastic reduction in measured sound speed.

Background noise's impacts questions the curve subtraction's success since it theoretically eliminates all noise present in both trials. Indeed, this foregrounded the tones excited by the tube, however, it is foreseeable that it would have also amplified any new reverberation by the geometric change. This likely included sound interactions between the chamber walls and tube (Johnston, 2009). The cardioid microphone, positioned slightly outside the tube, was sensitive to this laterally-approaching sound, being a random error source, although tube placement remained constant (Studiospares Europe Ltd, 2020) (Gallagher, 1999). Thus, inconsistent background noise, exemplified by the 8.0°C test, potentially impacted frequency analysis, hindering peak position confidence, and increasing frequency uncertainty.

Finally, temperature fluctuations during trials possibly allowed attribution of data to incorrect temperatures. These variations could have either occurred: across the entire system as it naturally returns to the room's temperature or; in different sections of the tube. The tube had one closed end, so although the fan hastened thermal exchange, some air in the tube may not have heated in time, altering the sound wave's identity within different tube segments.

9.2 Future Experimental Improvements

If this experiment were repeated, seeking more accurate results, certain alterations could improve data reliability. Primarily, were this experiment performed in an anechoic chamber, the harmonics yielded would more closely behave, reducing each sound speed's displacement from the literature curve. This study's chamber's imperfect performance served as systematic error for each harmonic. However, harmonic convergence has demonstrated that this expensive apparatus may not be necessary, replacing the cost with an additional data processing stage. Hence, while possible to rectify, this error is less important to consider.

Contrarily, the effect of external noise was significant. For example, to normalise the 8.0°C anomalous value, the refrigerator fan should be turned off, even with curve subtraction. Ideally, all prominent external sound should be eliminated, perhaps using a sound dampening room. Alternatively, hanging the microphone slightly inside the tube would reduce its inherent cardioid liability to external sound, while still creating potential reverberance geometry between microphone and internal tube surface, while using a more direct microphone could mitigate both errors and solely focus on sound propagated by the tube.

For temperature regulation, there were two issues: variation across the tube and; fluctuation during a trial. Solving the former, a two open-ended tube could be substituted, allowing better ventilation and faster temperature circulation. This only requires a slight alteration to the standing wave equation used (University of Tennessee, Department of Physics and Astronomy, 2020). Unfortunately, temperature fluctuations of the system are unpredictable, a major random error source. Its only control measures would be either using a better heat-insulated room or a continuous digital thermometer to track the exact temperature all throughout the trial, before strategically choosing the timestamps for frequency analysis.

10 Experimental Conclusions

10.1 Future Investigation and Academic Significance

This study recorded resonant frequencies and attributed them to sound speeds at various temperatures, confirming the well-known relationship, but also demonstrated how the influence of frequency on chamber performance could possibly be utilised to discover a value of theoretically perfect accuracy for the speed of sound using harmonic convergence. The most

important future investigation would be to confirm this by performing a similar experiment with a multi-harmonic focus as an independent variable, allowing the experimenter to attain results potentially as accurate as those from an anechoic chamber.

This experiment's academic significance is in its originality as an affordable environmental acoustics study which investigates temperature across multiple harmonics, allowing one to accurately quantify the relationship between dry air temperature and sound speed. Furthermore, since this was investigated through resonance, the chamber temperature's effect on the natural amplification of frequencies stresses the importance of real-world practices such as room tuning.

10.2 Conclusions

This investigation gave an alternative route into sound speed's calculation and its temperature reliance. This used wave speed's impact on resonance, so that analysis of a white noise broadband excitation of a constant length/diameter tube at different temperatures could indicate wave speed. An interesting conclusion tracked the acoustically dry chamber's performance across multiple harmonics to predict the true speed of sound when the chamber acts like a perfect anechoic chamber. Future research could see an experiment designed to confirm this trend, which promoted the possibility of an affirmative answer to the research question. This is true in that resonance has been shown to be able to confirm the trend of temperature against sound speed, but also multi-harmonic resonance has offered the opportunity to quantify this relationship accurately, even at a high school physics level with limited resources, making the data more accessible to a wider audience.

11 BIBLIOGRAPHY

Abom, M., & Allam, S. (2006). Investigation of damping and radiation using full plane wave decomposition in ducts. *Journal of Sound and Vibration*, 519-534.

Atkins, T., & Escudier, M. (2013). hydraulic diameter. In T. Atkins, & M. Escudier, *A Dictionary of Mechanical Engineering.* Oxford: Oxford University Press.

Audacity. (2020). *Free, open source, cross-platform audio software*. Retrieved from Audacity: https://www.audacityteam.org/

Bacon, M. E. (2012). Speed of Sound Versus Temperature Using PVC Pipes Open at Both Ends. *The Physics Teacher*, 351-353.

Bacon, M. E., & Torok, S. (2011). An Experimental Investigation of the End Effects for Blue Man Group® Pipes. *The Physics Teacher*, 152-154.

Boelkes, T., & Hoffmann, I. (2011). Pipe Diameter and End Correction of a Resonant Standing Wave. *International Scholastic Journal of Science*, 1-3.

Butterfield, A., & Szymanski, J. (2018). white noise. In A. Butterfield, & J. Szymanski, *A Dictionary of Electronics and Electrical Engineering (5 ed.).* Oxford: Oxford University Press.

Campbell, M. (2001). *End correction.* Retrieved from Oxford Music Online | Grove Music Online: https://doi-org.ezproxy.library.uq.edu.au/10.1093/gmo/9781561592630.article.49673

Crutchfield New Media, LLC. (2020). *QSC K10.2*. Retrieved from CRUTCHFIELD: https://www.crutchfield.com/S-TokcmfNHdnH/p_907K102/QSC-K10-2.html

Dalmont, J. P., Nederveen, C. J., & Jolly, N. (2001). Radiation Impedence Of Tubes With Different Flanges: Numerical And Experimental Investigations. *Journal of Sound and Vibration*, 505-534.

Desmos, Inc. (2020). *Let's learn together.* Retrieved from desmos: https://www.desmos.com/

Ellis, J. D. (2014). Superposition. In J. D. Ellis, *Field Guide to Displacement Measuring Interferometry* (pp. 8-8). SPIE Press.

Gallagher, M. (1999). Microphone polar patterns. *New York Vol. 25, Iss. 3*, 82-86.

Georgia State University, Department of Physics and Astronomy. (2016). *Speed of Sound in Air*. Retrieved from Hyperphysics: http://hyperphysics.phy-astr.gsu.edu/hbase/Sound/souspe.html

Georgia State University, Department of Physics and Astronomy. (2016). *Traveling Wave Calculation*. Retrieved from Hyperphysics: http://hyperphysics.phy-astr.gsu.edu/hbase/wavrel.html

Johnston, I. (2009). *Measured Tones | The Interplay of Physics and Music, Third Edition.* CRC Press LLC.

Kuttruff, H. (2016). *Room Acoustics (Sixth edition.).* Boca Raton: CRC Press.

Lytle, B. (2015, May). *Introduction to the Convergence of Sequences.* Retrieved from The University of Chicago | Mathematics: http://math.uchicago.edu/~may/REU2015/REUPapers/Lytle.pdf

Mitra, S. S., & Joshi, S. K. (1961). Thermal Expansion of Metals. *Journal of Chemical Physics*, 34-34.

Pushkarna, P. (2017). *An investigation into end corrections and open pipes.* Brisbane.

Rochman, D. (2017, August 10). *Mic Basics: What is Frequency Response?* Retrieved from SHURE | Performance and Production: https://www.shure.com/en-US/performance-production/louder/mic-basics-frequency-response

Schwinger, J., & Levine, H. (1948). On the Radiation of Sound from an Unflanged Circular Pipe. *Physics Review*, 383-406.

Studiospares Europe Ltd. (2020). *Rode NT5 Matched Pair*. Retrieved from STUDIOSPARES: https://www.studiospares.com/Microphones/Mics-Condenser/Rode-NT5-Matched-Pair_417110.htm#rtabs2

Thiel, J. (2006). *United States of America Patent No. US7003124B1.*

Tsokos, K. A. (2014). Standing waves in pipes. In K. A. Tsokos, *Physics for the IB Diploma, Sixth Edition* (pp. 185-186). Cambridge: Cambridge University Press.

University of Tennessee, Department of Physics and Astronomy. (2020). *Standing sound waves*. Retrieved from Physics 221, Elements of Physics: http://labman.phys.utk.edu/phys221core/modules/m12/Standing%20sound%20waves.html

Worland, R. S., & Wilson, D. D. (1999). The speed of sound in air as a function of temperature. *The Physics Teacher*, 53-57.